





## Observation of ion acceleration in nanosecond laser generated plasma on a nickel thin film under rear ablation geometry

Jinto Thomas ,\* Hem Chandra Joshi , and Ajai Kumar  
*Institute For Plasma Research, HBNI, Bhat, Gandhinagar, Gujarat 382428, India*

Reji Philip   
*Raman Research Institute, C.V. Raman Avenue, Sadashivanagar, Bangalore 560080, India*

 (Received 29 May 2020; accepted 3 September 2020; published 7 October 2020)

In this article we report acceleration observed for the ions produced in a 50-nm-thick nickel film coated on a quartz substrate, under nanosecond laser ablation, in the rear ablation geometry. A detailed study with varying background pressure and laser energy is done. Spectroscopic study including spectroscopic time of flight (STOF) measurements of ionic and other neutral transitions from the plasma has been undertaken. The STOF spectra recorded for ionic transition clearly show an enhancement in the velocity of the slow component as the background pressure increases. In addition, a large asymmetric spectral broadening in the 712.22-nm neutral line is observed, which increases with background pressure. While these observations have similarity to some of the reported studies on the acceleration of ionic species through double-layer formation, the electric fields calculated from the measured acceleration appear to be anomalously higher, and a double-layer concept seems to be inadequate. Moreover, the large asymmetry observed in the neutral line profile is indicative of microelectric fields present inside the laser produced plasma plume, which may play a role in the continuous acceleration of the ions. Interestingly, this asymmetry in spectral broadening exhibits temporal and spatial dependence, which indicates that significant electric field is present in the plasma plume even for longer duration and larger distance from the target. These spectroscopic observations of acceleration have also been complemented by triple Langmuir probe measurements. To the best of our information, such observations regarding large ion acceleration for the rather low laser intensities as used in this experiment have not been reported in literature so far.

DOI: [10.1103/PhysRevE.102.043205](https://doi.org/10.1103/PhysRevE.102.043205)

### I. INTRODUCTION

Laser-matter interaction has been an attracting subject because of its wide-ranging applications and fundamental interests. Applications of laser-matter interactions are elaborately described in a number of books and articles [1–5]. Particle acceleration using high-power lasers is one of the prominent applications of laser-matter interaction and an extensive study on laser-driven ion acceleration is available in literature [1,6]. Rajeev *et al.* demonstrated acceleration of neutrals to MeV energy for high intensity laser interaction in nanoclusters [7]. Interaction of intense laser pulses with ultra thin films resulting in acceleration of protons and ions has been experimentally demonstrated and simulated comprehensively by different groups [8–12]. Using high-intensity subpicosecond laser pulse and thin foil, forward ion acceleration due to electrostatic-field in nonequilibrium plasma has been reported by Maksimchuk *et al.* [13]. Bulanov *et al.* studied the use of intense proton beams produced by a high-intensity laser pulse for proton therapy [14]. Inertial confinement fusion [15] is a highly anticipated technological breakthrough of laser-matter interaction [16].

In laser-matter interaction, the kinetic energy acquired by electrons in the material is proportional to the laser intensity, and at higher intensities the energy transferred to the electrons will be of the ponderomotive energy [17–19]. Further increase in laser intensity produces relativistic electrons and can ionize other atoms in the lattice. When high intensity laser interacts with bulk samples, backward plasma acceleration (BPA) is observed, which can result in high ion yield [20]. At intensities above  $10^{15}$  W/cm<sup>2</sup> target normal sheath acceleration (TNSA) is reported [21,22]. TNSA can produce ions of the energies above MeV/charge state [22]. Unlike BPA, here the electric field is produced at the rear side of the thin target due to the escape of relativistic electrons. Another prominent acceleration mechanism is radiation pressure acceleration (RPA), which can accelerate the ions in excess of 10 MeV/charge state. However this requires an extremely high intensity of  $10^{19}$  W/cm<sup>2</sup> [23,24]. RPA is considered as the most effective mechanism for coupling laser energy to the target [24].

In most of the cases, ion acceleration has been observed in shorter pulse laser interaction with matter. Interaction of nanosecond laser pulse with matter and the formation and evolution of the plasma plume has been extensively studied by a number of groups [25–31]. However, most of these studies were centered at the plume expansion dynamics with different background species and background pressures with an objective to understand the physics behind plume dynamics in

\*jinto@ipr.res.in

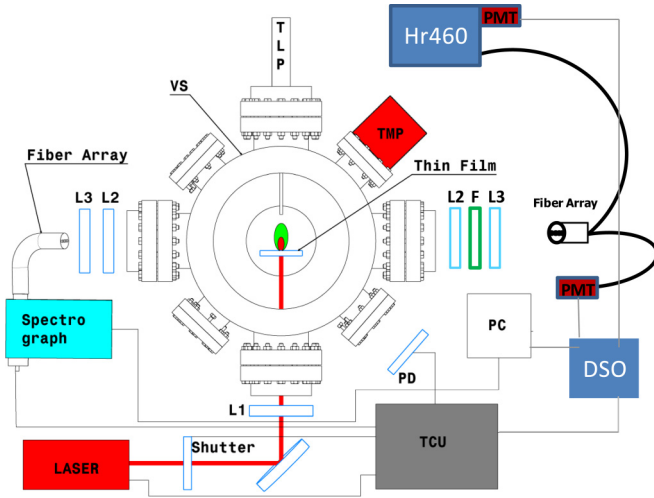


FIG. 1. Schematic diagram of experimental setup showing the arrangement of sample (thin film), triple Langmuir probe (TLP), and laser system aligned to the vacuum vacuum system (VS). TMP is the turbo molecular pump, L1 is the focusing lens, L2 and L3 are the lens system to image the plasma plume to fiber array. F is the band pass interference filter, Hr460 is the high-resolution spectrometer, PMT is the fast photomultiplier Tube, DSO is the fast digital storage oscilloscope, TCU is the trigger and control unit which synchronizes the instruments with laser pulses, and the data are acquired on a personal computer (PC)

pulsed laser deposition so that the film quality can be bettered [29–31]. Bulgakova *et al.* [28] observed ion acceleration in their experiment using ns laser pulses at a moderate laser fluence ( $2\text{--}25\text{ J cm}^{-2}$ ). This observation was explained by using the concept of self consistent electric field or widely known double-layer (DL) concept. In this work they concluded that the background gas suppresses the DL effect. They observed that the time-of-flight profile of the fast-ion peak gets modified with increasing background pressure depending on ion scattering by the background molecules and ion acceleration by the ambipolar electric field. Moreover, it was also found to depend on the distance from the target.

In this article, we report nanosecond laser produced plasma evolution in ambient  $\text{N}_2$  gas environment using optical emission spectroscopy (OES) and electrical probe, in rear ablation geometry, for a nickel film of 50-nm thickness, for laser fluences of 10 and  $21\text{ J cm}^{-2}$ . Time of flight profiles of OES indicate that ions are accelerated. However, the estimated electric field is anomalously higher and cannot be explained by the simple DL concept. Moreover, spectral line profile of the neutral nickel line ( $712.22\text{ nm}$ ) exhibits asymmetry which provides evidence towards the presence of microelectric fields and their contribution to the overall acceleration mechanism. In contrast to the reported observations of Bulgakova *et al.* [28], in this case ion acceleration appears to increase with background gases.

## II. EXPERIMENTAL SETUP

The experimental set up is similar to that described in an earlier work [32] and is shown in Fig. 1. Detailed description

of laser system, sample and diagnostics used in the study are described in the following sections.

### A. Laser system

The laser used for this experiment is 1064 nm Nd:YAG laser with  $\approx 8\text{ ns}$  pulse width, with Gaussian spatial profile (Continuum Powerlite 9030). Two laser energies 100 and 50 mJ are used for the experiment. The laser energy is measured using laser power meter and the energy on the sample is estimated after subtracting the reflection losses from the optical components. The laser is focused at the sample with a 50-cm plano convex lens and the spot size on the sample is  $\approx 1.1\text{ mm}$ , which is measured using a thermal burn paper on the spot. This results to the maximum energy density of  $\approx 21\text{ J cm}^{-2}$  and  $\approx 10\text{ J cm}^{-2}$  for 100 and 50 mJ, respectively. In rear ablation geometry, the laser is incident on the thin film from the rear side of the film through the transparent quartz substrate, and the plasma plume generated evolves in forward direction (direction of laser) as can be seen in the figure. The laser beam, sample manipulator, vacuum system, gas feed, etc., are the same as described earlier [32].

### B. Sample

Nickel film (50 nm thick) used in the present experiment is a commercially procured film coated by electron beam deposition method with roughly 5% variation in thickness. The film is almost completely ablated with single laser pulse itself and a precise high vacuum compatible sample manipulator is used to position the sample for the next pulse. The experiments are performed on single-shot basis and data from multiple shots with fresh sample positions are used to minimize statistical errors that may arise in the measurement.

### C. Diagnostics

(1) Spectroscopic time of flight (STOF) measurement: In this experiment, an imaging system with magnification 1 is used to image the plasma plume into an optical fiber array with 10 branches of fibers having core diameter of 400 microns each. The array is placed such that each individual fiber collects emission from various spatial locations from the sample along the axis of the laser beam. Any fiber from this array can be coupled to a PMT so that recording of emission from different positions within the plasma is possible on a shot-to-shot basis. Narrow bandpass interference filters (F as shown in figure) with pass band for prominent neutral nickel lines are used to allow the desired line emission to reach the PMT. The PMT coupled with a fast digital oscilloscope (DSO) records the temporal emission of the respective neutral lines from the respective locations. It is possible to couple any of the remaining fibers from the fiber array to another spectrometer (HR460), which is equipped with a PMT. This spectrometer and PMT combine are used to detect ionic spectral lines from the plasma. The spectral resolution of this spectrometer with PMT is around 0.1 nm. The spectrometer is arranged with an F number matching optics for the SMA fiber.

(2) Spectral line profile measurement: A 1-m spectrometer is also coupled with another fiber array with 10 fibers using F number matching optics to record the spectra of plasma. The

TABLE I. Spectroscopic details of lines used in the present study [33].

Lambda (nm)	Aij ( $10^7 s^{-1}$ )	J —	Ej (eV)	Ei (eV)	Transition
361.94 Ni I	6.6	3	0.42	3.85	$3d^9(^2D)4p \rightarrow 3d^9(^2D)4s$
362.68 Ni II	—	5	0.19	3.60	$3p^63d^8(4s) \rightarrow 3p^63D^9$
508.11 Ni I	5.70	7	3.85	6.29	$3d^9(^2D_{3/2})4d \rightarrow 3d^9(^2D)4p$
712.22 Ni I	2.10	3	3.54	5.28	$3d^9(^2D_{3/2})5s \rightarrow 3d^9(^2D)4p$

fiber array is placed at the image plane of another imaging system aligned diametrically opposite to the earlier mentioned fiber array so that emission from the plasma along the propagation axis can be imaged to the spectrometer. The slit of the spectrometer is fixed at 50 microns so that an effective spectral resolution of 0.12 nm is achieved. The spectrometer with fiber array and ICCD enables acquiring spectra from different locations of plasma plume simultaneously and for different time delays on a shot to shot basis.

(3) Triple Langmuir Probe (TLP) measurement: In addition to the spectroscopic diagnostics, TLP is also used for the measurement of floating potential and ion current. TLP records the ion saturation current and floating potential at a distance of 10 mm onwards. It can be noted here that the emission spectra from ions and neutrals are recorded at the locations closer to the sample whereas ion saturation current and floating potential from 10 mm onwards as it is not possible to put the probe closer to the target. The signals from PMT's and TLP are recorded using the DSO which is synchronised with the timing control unit (TCU) and interfaced to the PC.

#### D. Spectral lines

Table I lists the transition details of different spectral lines used for the present study. STOF studies for Ni II 362.68 nm and neutral Ni I 361.94 nm, 508.11 nm and 712.22 nm nickel lines are used to study the temporal evolution of the respective species. Spectral line shape of the 712.22 nm Ni I line is also studied, for which a large asymmetrical spectral broadening is observed. None of the spectral lines used in the present work involve ground state. Though the lower level of the 362.68 nm Ni II line is closer to the ground state (0.19 eV), the present measurement can be considered free of self absorption because of the low density of the species (neutrals/ions) in plasma for the temperature and density range relevant for 100 ns delay from the laser pulse [32].

### III. RESULTS AND DISCUSSION

The acceleration of ionic species is primarily observed in the STOF data of the ions. Along with STOF, spectral line shape of neutrals line (712.22 nm) and TLP data have been used to explain the observed results. The section is further divided in four subsections.

#### A. Acceleration of ions

In this section, STOF data of the ionic and neutral species of nickel are discussed. A clear dependence of the temporal evolution between ionic and neutral species on the ambient pressure is observed.

Figure 2(a) shows the STOF emission recorded for the ionic line 362.68 nm of nickel at 3 mm from the sample for different background pressures, at a laser energy of 100 mJ. The figure shows that the evolution of the slower peak becomes significant as the background pressure increases from 0.1 to 20 mbar. At 0.1 mbar, the slower peak is not evident as can be seen from the figure. However, it appears with the same intensity as that of the faster peak when the background pressure reaches 5 mbar, and the intensity increases substantially with further increase in pressure. Further, it can be noted that the slower peak gradually advances in time as the background pressure increases. A closer look at the faster peak shows an interesting behavior. The faster peak appears at the same time

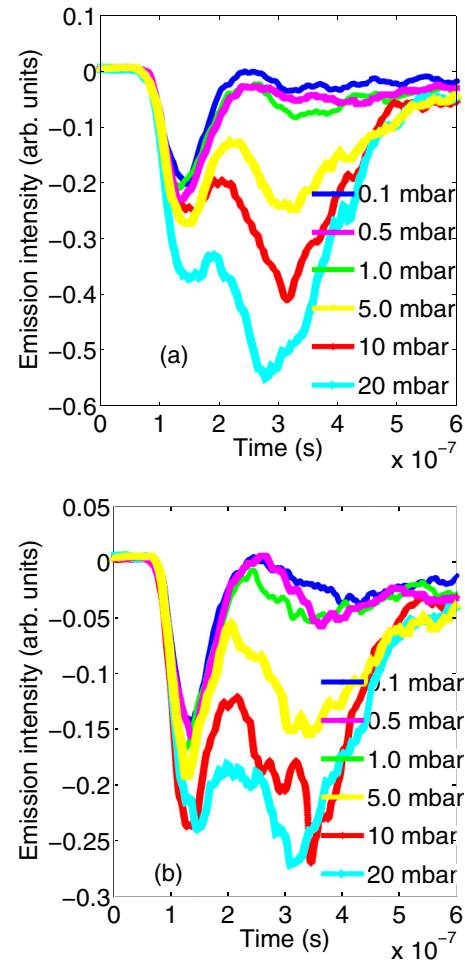


FIG. 2. Evolution of STOF spectrum of ionic line (362.68 nm) at 3 mm from the sample for different background pressures for 10 ns, 1064 nm laser pulse at laser energies of (a) 100 mJ and (b) 50 mJ.

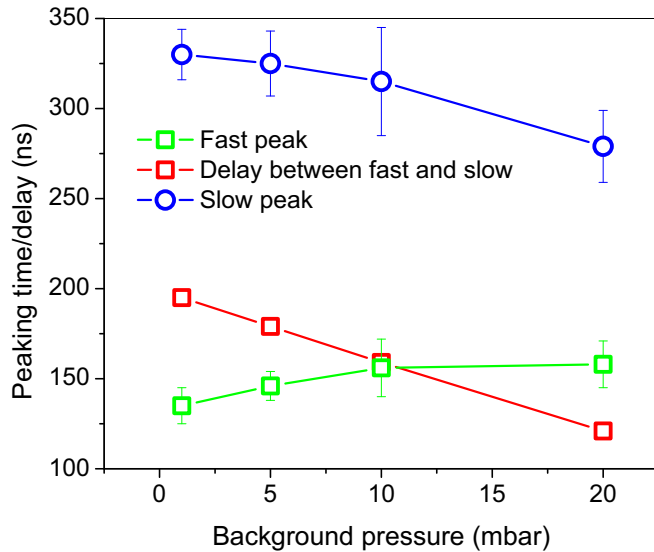


FIG. 3. Peaking time of fast and slow peaks of STOF spectra of ionic species and the delay between fast and slow peaks with varying pressures for 1064 nm laser wavelength with 100 mJ of energy at 3 mm from sample.

up to a background pressure of 1.0 mbar. However, it slows down marginally as the pressure increases further (Fig. 3). A similar trend is seen in the STOF spectra of ionic species with 50 mJ laser energy, as shown in Fig. 2(b). The slowing down of the faster peak can be understood as a consequence of collisions between fast ions with the background gas molecules as described in earlier studies [29–31]. It is interesting to see that the temporal separation between the faster and the slower peaks decreases from 195 ns at 1 mbar background pressure to 120 ns at 20 mbar background pressure, when ablated with 100 mJ of laser energy (Fig. 3). In case of ablation with 50 mJ laser energy, the separation changes from 220 to 150 ns in the same range of background pressure. From STOF spectra it can be noted that the intensity of the fast peak is not affected much by the background pressure, while the slow peak shows an enhanced intensity and increase in velocity. This observation can be used to rule out the possibility of splitting of the faster peak due to multiple collisions with the background gas as reported in some of the earlier studies [34,35]. The fast peak is apparently due to the ions that penetrate the ambient whereas slow peak due to the ions that are confined by it [34,36]. In these studies it is clearly observed that the fast peak is not much affected by the increase of background pressure but the slow peak further slows down significantly as the background pressure increases [29,36,37]. The striking difference observed between the present and earlier reported works is probably because of the configuration of ablation (rear versus front ablation geometries). It is interesting to note that at lower laser energy (50 mJ), the slow peak of ionic emission is more prominent at lower background pressure (0.1 mbar). In comparison, at higher laser energy (100 mJ) there is no significant intensity for the slow peak. The intensity of ionic line is higher for higher laser energy. On plume splitting, earlier works [36] reported that the fast peak is not significantly retarded with increase in background pressure. However, the emission

intensity decreases significantly with increase in pressure. However, the slow peak is significantly retarded with increase in background pressure. In our observation also the fast peak is not retarded much with increase in background pressure. However, a contradictory behavior is seen for the intensity of fast peak, which increases with background pressure. Another important observation from the STOF spectra of ionic species for various background pressures and laser energies is that the velocity of the slow component gets increased with background pressure and laser energy. For instance, the fast peak gets slowed down whereas the slower peak becomes faster with pressure as can be seen in Fig. 3. Though it is not clear why the slow peak becomes faster, the slowing of the fast peak can be attributed to enhanced collision with the ambient, leading to a reduction of its momentum [29]. Further, it is interesting to see that the fast peak has relatively higher intensity for 50 mJ energy. Normally it is expected that more charged species are present at higher energy. This anomalous observation appears to be due to the screening of the ions and hence decreased acceleration.

Akin to the ionic spectra, emission spectra of neutrals are also recorded using the same configuration, by changing the central wavelength of the spectrometer to three prominent neutral nickel lines as listed in Table I. Figure 4 shows the STOF emission of all the three neutral lines recorded at 3 mm from the sample for both laser energies. As can be seen from the figure, for particular laser energy and pressure, the 361.94 nm neutral line peaks faster than the other two lines (slow peak). The neutral lines 508.11 and 712.22 nm show a similar trend in peaking time for the slower peak. Both lines have lower intensity. However, fast peak for 712.22 nm line [Figs. 4(c) and 4(f)] has relatively higher intensity. As the background pressure increases, the intensity of slower peak increases significantly whereas the intensity of faster peak decreases slightly. However, 361.94 nm neutral line does not show any trace of fast peak for both laser energies at this distance. The neutral lines show that the peaks get slightly delayed with increase in the background pressure. For the 361.94 nm emission, as can be seen from Fig. 4(a), the peak position does not change significantly as the pressure increases from 5 to 20 mbar. However, for the other two lines the peak position delays gradually with increase in background pressure [Fig. 4(b) and 4(c)]. The variation observed in the dynamics of different neutral species is interesting and it has to be noted that the intensity of a particular spectral transition depends on recombination/excitation, and hence on plasma parameters (density and temperature), as well as on the properties of the specific transition.

From the observation of the STOF profile of ionic and neutral lines of nickel at 3 mm in this experimental configuration, it is clear that the ionic species within the plasma have significantly higher velocities in comparison to neutral species. Also, the velocity of ionic species increases with increase in background pressure which is worthwhile to note because instead of getting slowed down due to resistive force of the medium, ions get accelerated. This may probably be due to increase in electron density and subsequent increase in electric field, as will be discussed later. Figure 5 shows the peaking time of the slower component for ionic emission and for neutral lines for varying background pressures at

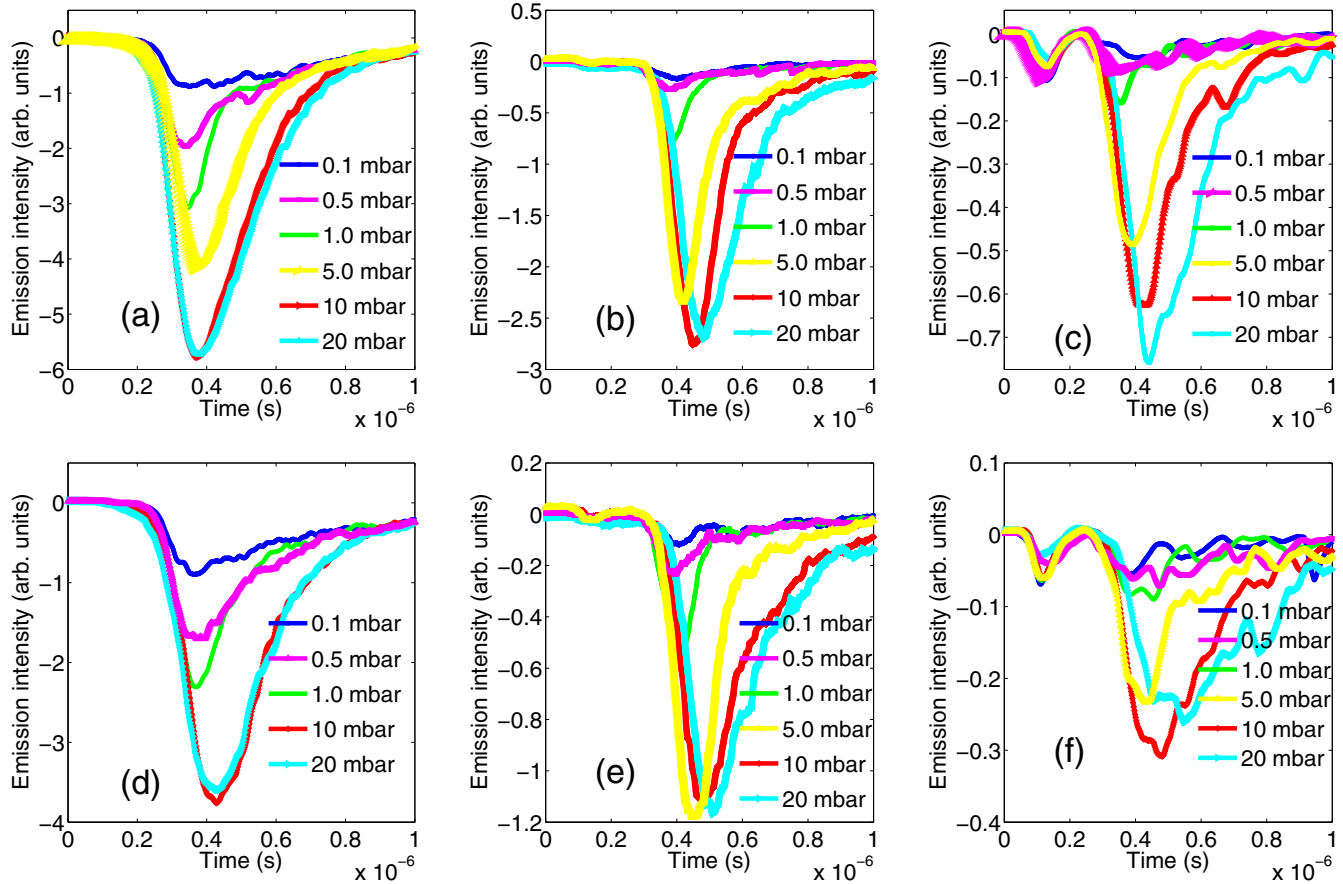


FIG. 4. Evolution of STOF spectrum of neutral lines 3 mm away from the sample for different background pressures and laser energies 100 mJ (a)–(c) and 50 mJ (d)–(f) for 10 ns, 1064 nm laser. The neutral lines are 361.94 nm (a), (d), 508.11 nm (b), (e), and 712.22 nm (c), (f).

100 mJ laser energy at 3-mm distance. The peaking time and its variation with background pressure are distinctly different

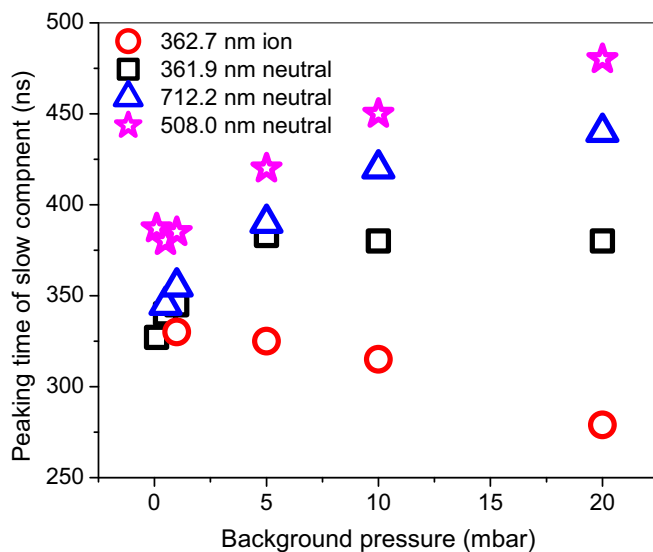


FIG. 5. Comparison of peaking time of slow components of STOF spectra of ionic and neutral species with varying background pressure for 1064 nm laser wavelength with 100 mJ of energy at 3 mm from the sample.

for ions and neutrals. For ions, as the pressure increases, the slow peak gets faster. However, this is not the case for neutral lines. The 361.94-nm line shows that the pressure does not affect the peaking time as background pressures increases (from 5 mbar to 20 mbar the peaking time remains almost constant as can be seen from the Fig. 5). However, the other two neutral emission lines (508.11 and 712.22 nm) show that the peaks slow down further as the pressure increases. As the peaking time for ions as well as the neutrals is almost same at lower pressures (Fig. 5), it can be assumed that the neutrals are initially formed from the ionic species closer to the sample. With increase in background pressure neutrals are affected only by a small degree, whereas the velocity of the ionic species increases with pressure. However, as the role of background gas is same for the neutrals and ions, it has to be assumed that the ions get some additional acceleration as the pressure increases, so that they gain velocity. As mentioned earlier, it can be assumed that part of the neutrals may be formed from the recombination process in ionic species and may continue with initial energy they acquire from the ion until the gas pressure drags them and slows it down. Earlier studies have demonstrated the effect of background pressure, laser energy and dependence of spatial location on plasma plume splitting in LPP (backward ablation) geometry. Some studies show a completely different behavior as expected for plume splitting and propagation. For instance, the dynamics of carbon plume in helium background [35] has shown that

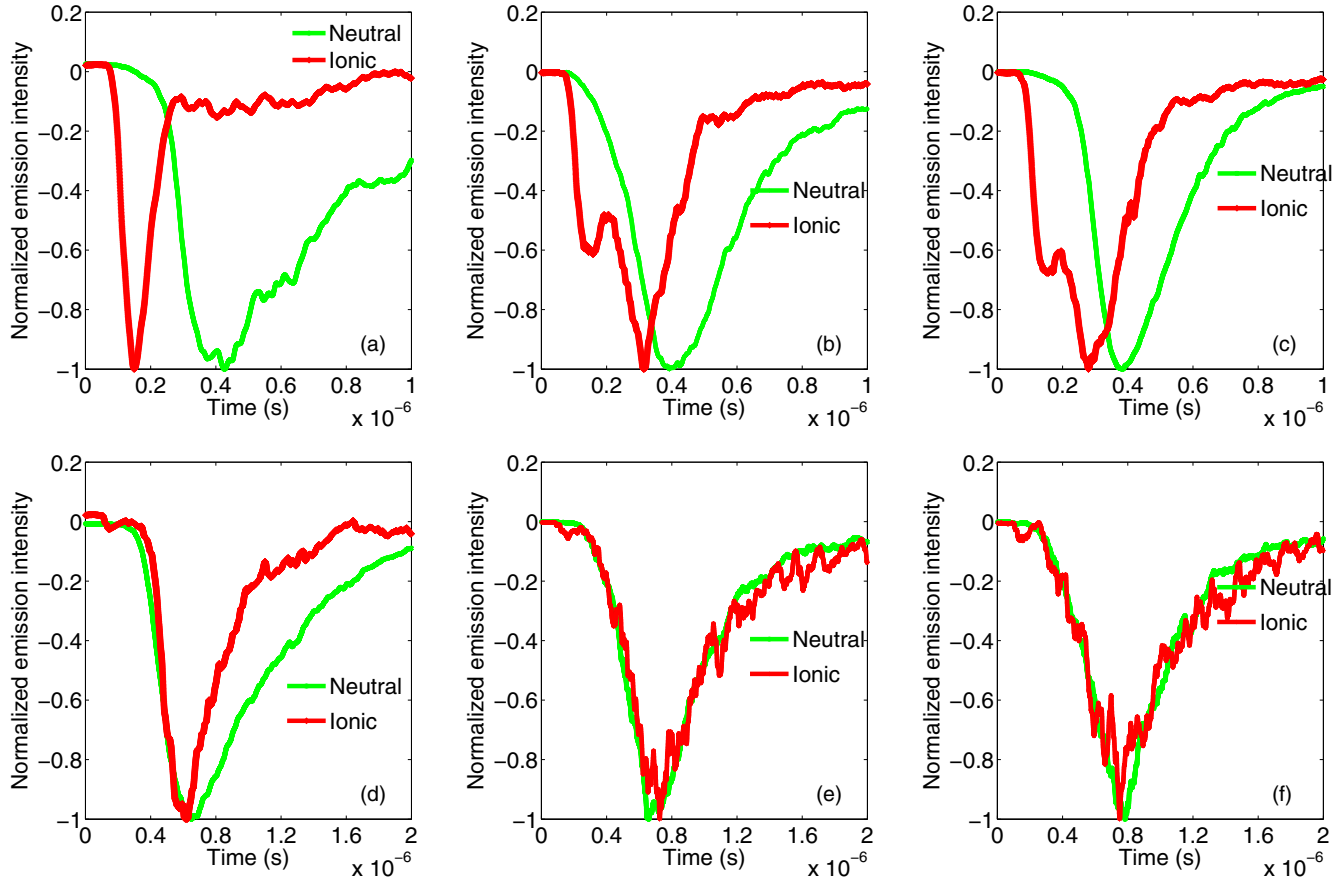


FIG. 6. Temporal evolutions of neutral (361.94 nm) and ionic (362.68 nm) lines at 3 mm (a)–(c) and 7 mm (d)–(f) for different background pressures for laser energy of 100 mJ. The background pressures used are 0.1 mbar (a), (d), 10 mbar (b), (e), and 20 mbar (c), (f).

the fast peak gets slowed down as the laser irradiance is increased. It is also mentioned that the velocity of fast peak increases and that of the slow peak decreases as the helium pressure increases. The observation of decrease in the velocity of the faster component with increase in laser irradiance has been explained as a selective depletion of high velocity C<sub>2</sub> species. The effect of background pressure on the velocity of faster peak is explained using the inverse relation of pressure and energy in the adiabatic expansion model [35]. We would like to mention that the present results also exhibit a totally unexpected nature in the behavior of the slow peak.

The behavior of the ionic (362.68 nm) and neutral (361.94 nm) lines at 7-mm distance were also recorded by using the optical fiber coupled to spectrometer and PMT. For an easy comparison of the differences in STOF of neutral and ionic lines at 3 and 7 mm, the STOF spectra with sufficient visibility are shown in Fig. 6 for 100 mJ energy. The figure shows a single peak for neutral emission, but distinctly two or more peaks for the ionic line (specifically at 3 mm). Hereafter the peaks will be denoted as: (i) fast ion peak, (ii) slow ion peak, and (iii) neutral peak for further discussion. The maximum intensity of each emission line is normalized to 1 for ease in comparison. Though the ionic and neutral lines (362.68 and 361.94 nm) are separated by 0.8 nm, the resolution of the spectrometer is sufficient enough to resolve them. At 3 mm, as can be seen from Fig. 6, single peak corresponding to ion is observed at lower pressure. With increase in pressure, double

peak structure emerges with both fast and slow ion peaks. However, for neutral emission a broad single peak is observed which becomes sharper with increase in pressure. The results indicate that the fast ionic peak should come from accelerated ions whereas the slower peak may result from the drag exerted by ambient pressure. As the neutral peak is delayed even with respect to the slow ionic peak, it appears that neutral emission indeed comes from the neutrals directly produced in the ablation process. It can be noted that the fast neutral peak appears with considerable intensity for other wavelengths [particularly 712.22 nm as shown in Fig. 4(c)] which is again interesting that at 7 mm the scenario is changed completely. A single peak corresponding to ion is observed which corresponds to the slow ionic peak. However, the neutral emission profile slightly differs from the ionic profile at low pressures but completely matches with ionic profile at higher pressures. This indicates that at this distance almost all the neutrals are produced by the recombination process, which is enhanced at higher background pressures. At longer distances as temperature decreases, it will subsequently increase recombination. It also shows that the neutral peak is broader than the ionic peak, especially at lower background pressure. It is likely that neutrals may originate from recombination process from ion as well directly formed in the ablation process. This can explain rather broad distribution of neutral STOF spectrum. It can be noted that at lower fluence also, similar behavior in the STOF of ionic and neutral species is observed. Figure 6

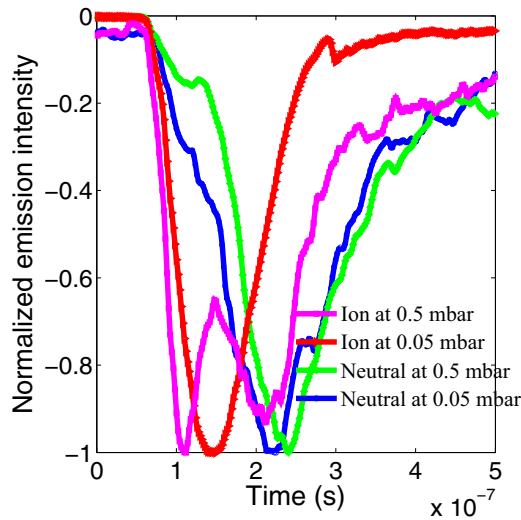


FIG. 7. Temporal evolution of STOF spectra of ionic and neutral lines (362.68 and 361.94 nm) for two background pressures for 1064-nm laser wavelength with 50 mJ of energy at 0.5 mm from the sample.

shows that the ionic peaks get accelerated as the background pressure increases.

The striking differences between ionic and neutral STOF and their spatial dependence are quite interesting and prompt to the analysis of data collected from even closer distances from the film  $\approx 1$  mm. However, very close to the sample the emission intensity of the ionic component (corresponding to 362.68 nm) is less and it becomes unobservable as the background pressure increases. Using the same spectrometer and PMT set up, the ionic and neutral line behavior is recorded for  $5 \times 10^{-2}$  mbar and  $5 \times 10^{-1}$  mbar. For recording the emission behavior of neutral lines listed in Table I at a closer distance, adjacent fibers separated by less than 1 mm are used. The fiber closer to the sample is used with spectrometer and PMT to record the signal within 1 mm from sample. Spectra from the other fiber are recorded using interference filters for respective neutral lines and PMT. The signals are recorded for different background pressures and laser fluence. The plasma plume is imaged using an imaging system and fiber array as described earlier. In Fig. 7, the effect of background pressure on ionic (362.68 nm) and neutral (361.94 nm) line for background pressures of  $5 \times 10^{-2}$  mbar and  $5 \times 10^{-1}$  mbar is shown. The intensity of ionic emission is low and hence higher gain for the PMT is used. The STOF spectrum is normalized with maximum intensity for each spectrum. As can be seen from the figure, the ionic emission is faster than the neutral emission for both the pressures. As the background pressure increases from 0.05 to 0.5 mbar the neutral STOF shows slight drag whereas the ionic line shows a double peak structure and the fast peak of ion advances ahead of the ionic peak observed at low pressure. The behavior of fast peak of ionic line is similar to what is observed at 3 mm. At lower pressure fast and slow components appear to be merged together which, however, clearly separate at higher pressures. It may also be noted from the figure that even the neutral spectra at 0.5 mbar show an onset of a fast peak at around 120 ns, which is

prominent at higher pressures. As discussed earlier, fast ionic peak comes from the acceleration process. Small hump in the neutral STOF may be due to recombination of the fast ions.

Figure 8 shows the STOF spectra for three different neutral lines (361.94, 508.11, and 712.22 nm) using the same optical fiber and PMT for different background pressures. As can be seen from Fig. 8(a), for all the three pressures, the STOF spectra show two well-resolved peaks for 50 mJ energy. It can be noted that the neutral emission spectra recorded by spectrometer (Fig. 7) do not show well resolved peaks as seen here at the same energy, which may be due to smaller distance from the target (less than 1 mm). Interestingly, the slower peak becomes faster (observed at shorter time) as marked in the figure and the faster peak gets slightly slowed down as the pressure increases from 0.1 mbar to 10 mbar, showing similar behavior as that exhibited by the ionic line. The slower peak at 305 ns for 0.1 mbar advances to 265 ns by increasing the background pressure to 10 mbar. At the same time, the faster peak trails from 140 ns to nearly 160 ns. Although this 20 ns variation is rather small and may be argued as uncertainty, it should be noted here that triggering of acquisition is done by a fast photo diode of 1 ns rise time and every component used in this experiment like PMT, filter, cables, and triggering mechanism are exactly the same. Moreover, the emission earlier to the fast peak due to laser line leak matches well and hence timing is not a matter of concern. Figures 8(b) and 8(c) are the evolutions of STOF spectra of 508.11 and 712.22 nm, respectively, which show distinctly different temporal behavior, as compared to 361.94 nm. The fast peak for 361.94-nm emission shows enhancement with increase in pressure, for 508.11-nm line there is no significant enhancement, and for 712.22-nm line there is an appreciable decrease in intensity. However, for the slower peak there is enhancement in the intensity for all the three lines. The 508.11-nm emission has significantly low intensity for the fast peak even at higher pressures in comparison to the slow peak. However, the STOF spectrum of 712.22 nm shows significant intensity for the fast peak for all the three background pressures. From Fig. 8 it is evident that the slower peak of 361.94 nm advances significantly with pressure but the other two neutral lines do not show as much variation as that in case of 361.94 nm. It is likely that the governing atomic processes, e.g., recombination process for these three transitions get modified distinctly for the different transitions resulting in different behavior for the corresponding neutral lines. It can be noted that transition probability (Table I) for 712.22-nm line is lowest, but still it is prominent. This clearly indicates that recombination process has highest contribution for this line. Thus it can be understood that the faster peak which is created by recombination process in the ions shows up with highest intensity in case of 712.22-nm line. This is also supported from the results of Fig. 4.

We recorded the STOF spectra for these lines at higher energy of 100 mJ also, which is shown in Fig. 9. For this laser energy, in the case of 361.94-nm emission, the slow and fast peaks appear merged together as can be seen in Fig. 9(a). The peak position advances significantly to 210 ns for 10.0 mbar background pressure. This again indicates that the fast peak gets slowed down and the slower peak gets accelerated. As a result the peaks appear merged. From a closer look at the figure, it can be inferred, though distinctly, that for 1.0 mbar a

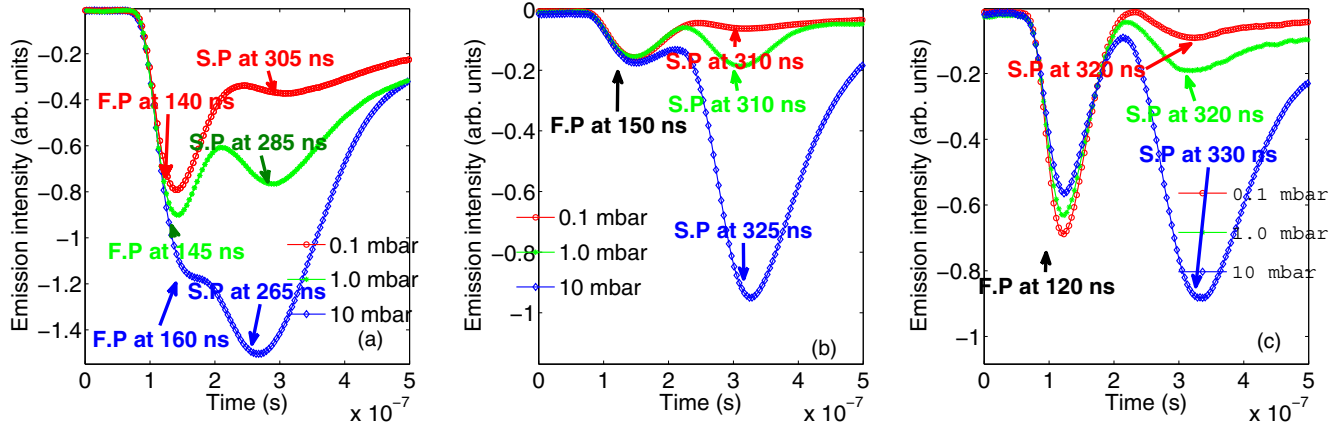


FIG. 8. Temporal evolution of neutral lines 361.94 nm (a), 508.11 nm (b), and 712.22 nm (c) of nickel at very close (1 mm) to the sample for 1064-nm laser ablation using 50 mJ energy. F.P. is for fast peak and S.P. for slow peak.

slower peak appears at a later time nearly 260 ns. Figures 9(b) and 9(c) show STOF spectra of 508.11 and 712.22 nm, respectively, where no significant deviation in evolution pattern or peak position is observed in comparison to the STOF spectra observed at 50 mJ (Fig. 8). However, the emission intensity is increased significantly for both these lines as compared to the 50 mJ excitation.

As mentioned earlier the dynamics of emission spectra of different transitions are slightly different, but it shows a consistent double peak structure for all the transitions. The 361.94-nm neutral emission shows a trend similar to the ionic spectra recorded for different pressures, i.e. as the background pressure increases, the second peak advances. Hence, the assumption of evolution of neutrals from the ions appears to be quite reasonable. These observations also highlight the role of particular atomic transition for observing the fast peak using optical time of flight measurements.

**B. Loss of electrons from plasma at initial stage charge separation in plasma plume similar to double layer formation**

The neutral and ionic emissions observed at different locations clearly show an enhancement in the velocity of slower

component of ions and some specific neutral species up to a certain distance. To extract more information we have used TLP to observe behavior of ions as well as the evolution of potential inside the plasma. However, it is not feasible to make any measurements close to the sample considering the rather high plasma density and temperature [38,39]. Hence, for ascertaining the dynamics of the ions, TLP measurements have been used beyond 10-mm distance from the target.

Figure 10 shows the evolution of ion saturation current recorded using TLP at 10 mm from the sample for different background pressures for both the laser energies. It is interesting to monitor the evolution of ion saturation current considering the observation of STOF spectra of ionic species, where the slower component advances in time with background pressure. However, no such observation is seen in the evolution of the ion saturation current at 10 mm from the sample. Instead, it slows down with background pressure. The ion saturation current shows that there may be multiple components of ionic species present as distinct peaks. As the ion saturation current is measured at a longer distance from the target, variation from STOF results is expected.

It can be noted that the position of the first peak of ion saturation current for low background pressure (0.1 mbar) is

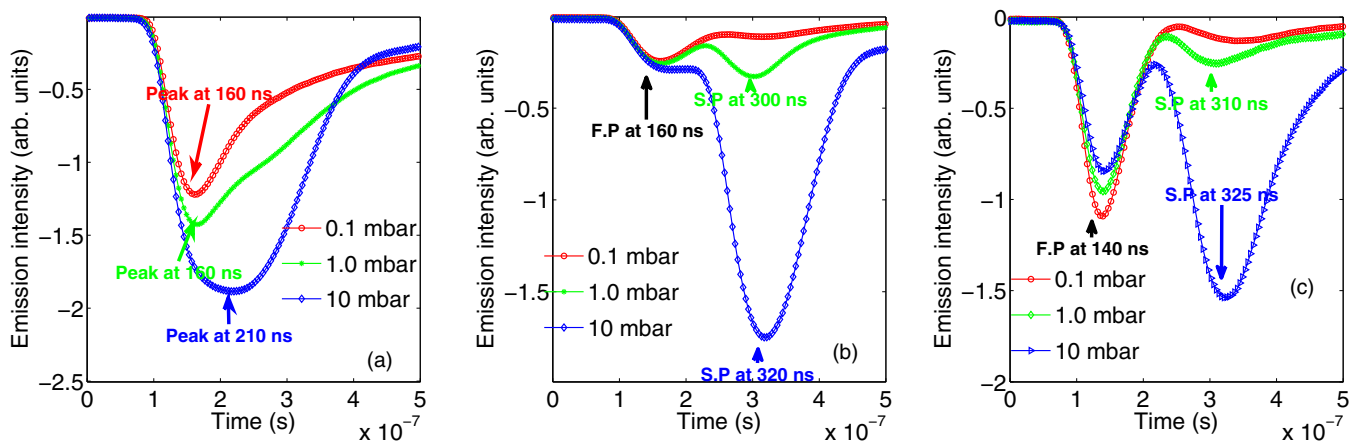


FIG. 9. Temporal evolution of neutral lines 361.94 nm (a), 508.11 nm (b), and 712.22 nm (c) of nickel at very close (1 mm) to the sample for 1064-nm laser ablation using 100 mJ energy. F.P. is for fast peak and S.P. for slow peak.



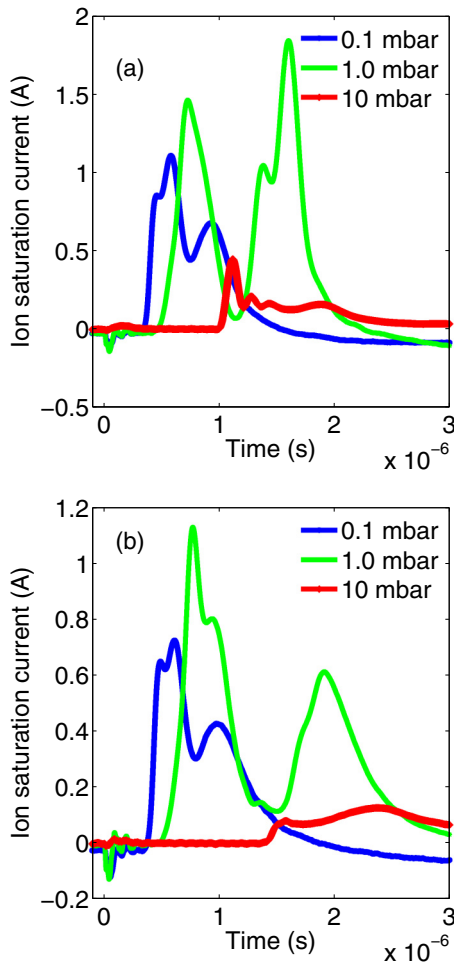


FIG. 10. Temporal evolution of ion saturation current at 10 mm from the sample for different background pressures and laser energies of (a) 100 mJ and (b) 50 mJ.

not largely different for both the energies. For instance, at 0.1 mbar, the ion saturation current peaks at 452 and 490 ns for 100 and 50 mJ, respectively. The second peak of ion saturation current is observed at 584 and 616 ns, respectively. At 1.0 mbar the first peak is observed at 730 and 770 ns for 100 and 50 mJ, respectively. However, at 10 mbar, first peak for 100 mJ ablation is significantly faster (1120 ns) compared to the peak (1510 ns) for 50 mJ. A straightforward comparison among other peaks is difficult as the peaks are not distinctly visible at many instances. At this stage, it is interesting to point out that at low pressure (0.1 mbar), the velocity of the fast peak (at 135 ns Fig. 3) for ionic line at 3 mm can be correlated with that of the fast peak [which is not well separated at 435 ns, Fig. 10(a)] observed for ion saturation current at 10 mm. However, the velocity corresponding to the ionic emission at 7 mm (at 600 ns) does not match these velocities. Instead, it is comparable to the slowest peak (at 950 ns) observed for ion saturation current. Hence, at lower pressure the optical STOF measurement and the TLP measurements are reasonably correlated. The first and last peaks of ion saturation current at 10 mm from the sample and at background pressure of 0.1 mbar and laser energy of 100 mJ [Fig. 10(a)] match with the STOF recorded for ionic species

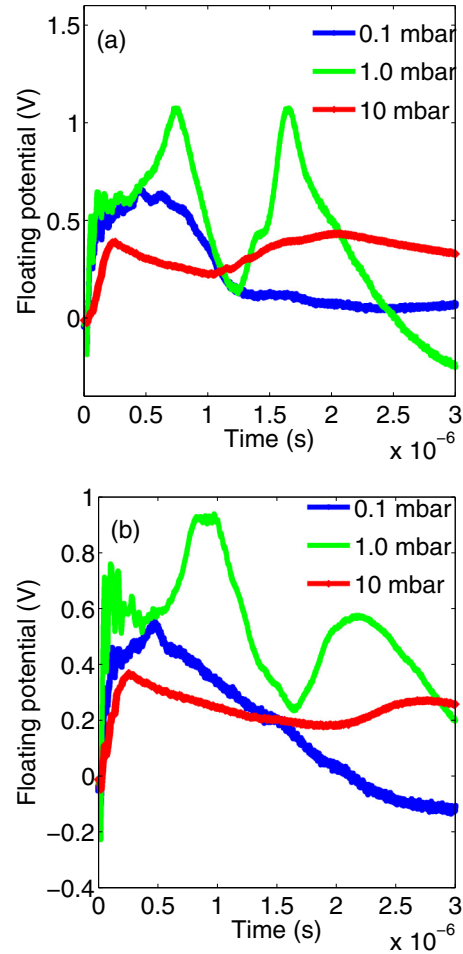


FIG. 11. Temporal evolution of floating potential at 10 mm from the sample for different background pressures and laser energies of (a) 100 mJ and (b) 50 mJ.

at 3 and 7 mm. This correlation between two measurements is interesting and confirms that ionic species do not undergo any significant drag at lower background pressures. Here it has to be noted that the fast peak of neutrals and ions show a slight drag at higher background pressure, in contrast to the slow peak, which advances significantly with increase in background pressure. This may be due to an interplay between the drag offered by the background and the acceleration obtained from plasma. The initial enhancement in velocity of fast ionic peak, which subsequently becomes slower as the pressure increases confirms the possibility of such interplay.

Figure 11 shows the temporal evolution of floating potential recorded at 10 mm from the sample along with the ion saturation current using the TLP. Here, the floating potential shows immediate response to the laser interaction with the sample (within 10–20 ns of laser incidence) which shows a fast rise in floating potential at a time where the fast negative current is observed in ion saturation current. The floating potential in the plasma can provide insight into the electron temperature at the particular location. However, it should be noticed that in this case the TLP is at a distance of 10 mm from the sample. It is possible to rule out the plasma generated on the sample (thin film) by the laser pulse reaching the probe

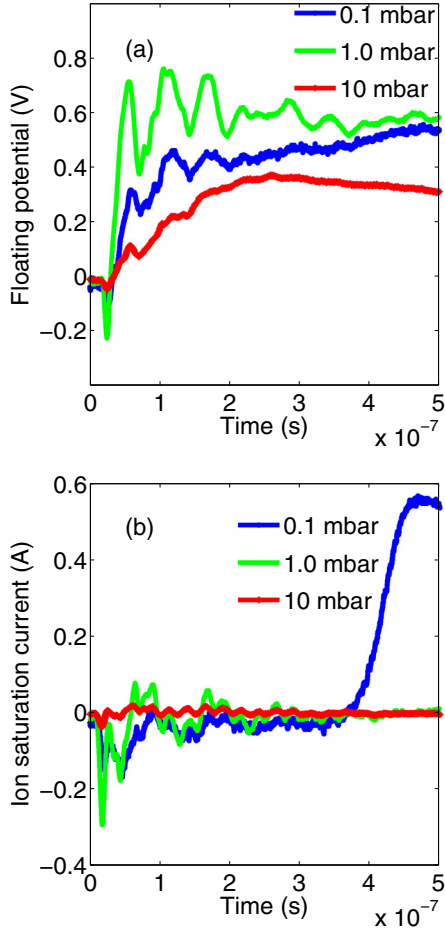


FIG. 12. Zoomed section of the floating potential (a) and ion saturation current (b) recorded at 10 mm away from sample at early stages of plasma plume for 50 mJ energy, showing the traces of oscillations.

location within 10 ns. Hence, the potential recorded on the TLP appears to be due to some other mechanism. Zoomed views of floating potential and ion current at the early stages of plasma are given in Fig. 12. The figure shows well-defined damping oscillations in floating potential as well as some non-periodic negative peaks in ion saturation current at early stages (10 to 25 ns) of the plume evolution. Negative value of ion saturation current shows that the contribution to the current is due to electrons. Moreover, the peaking time of the negative peak is not affected by the background gas pressure unlike ion saturation peak, which significantly gets delayed as the background pressure increases. Here it has to be mentioned that the probes are biased over  $-20$  V for measuring the ion saturation current and electrons with energy higher than 20 eV is reaching the probe to record the negative current. These electrons interact with the background gas and ionize it, as seen from earlier studies [36]. The negative values of ion saturation current and the detection of potential by TLP shows the ejection of electrons from the initial plasma formed from the sample. The possible cause of generation of hot/fast electrons will be discussed later. However, at this instant, the reason for oscillations observed on the floating potential does not have a clear-cut explanation. Oscillations in ion saturation

current for laser-plasma were also reported earlier [40], which are usually explained by plasma double-layer effects. Gurlui *et al.* [40] further analyzed these oscillations and concluded that it might be due to the self structuring of the interface of double layers coupled with temperature fluctuations.

For some other instances, the occurrence of such fast response on probes is attributed to prompt electrons due to photoionization by the stray laser photons (reflections from the sample) on the probes. However, in this case, the photon energy is significantly low for photoionization to occur. In addition to this, due to the configuration (rear ablation geometry) of the experiment laser photons cannot reach the probe as the film is opaque. The assumption of opaqueness of the film during the entire laser duration may have some fall outs considering the fact that the trailing part of laser pulse sees nickel plasma rather than the film itself. For 1064 nm, estimated critical density ( $n_c$ ) comes out to be  $\approx 8.8 \times 10^{20} \text{ cm}^{-3}$  ( $n_c = \frac{\omega^2 m_e \epsilon_0}{e^2}$ ), where  $\omega$ ,  $m_e$ ,  $\epsilon_0$ ,  $e$  are the laser frequency, mass of electron, permittivity of free space, and the charge of electron, respectively). As the nickel density is of the order of  $10^{23} \text{ atoms/cm}^3$ , even a small percentage (2%) of ionisation can result in the density to be beyond critical density. As mentioned earlier, IB is likely to happen in the initial stages of the plasma when density is expected to be greater than the critical density hence for the trailing portion of laser, it becomes opaque. Hence, leaking of laser photons can be ruled out. Further, it can also be noted that the ambient pressure dependence which is observed in the early stages of TLP signals (Fig. 12) also confirms that the cause of this should not be the laser radiation or the light emission from the nascent plasma (not likely to affect the probe as it is not intense enough). The onset of negative peaks and oscillations in the ion saturation current and floating potential may be assumed due to the interaction of fast electrons generated from the laser interaction with nickel film. The decrease in the influx of electrons at higher pressures may be due to increased number of collisions with the background gas. It is well known that the electron-neutral collision rate is a function of the number density of the background gas molecules and the temperature (velocity) of the electrons. For instance, for electrons with velocity equivalent to 3 eV at a background gas pressure of 0.1 mbar, the collision rate is estimated of the order of  $10^{12} \text{ s}^{-1}$ , which increases by two orders of magnitude when background pressure increases to 10.0 mbar.

The observation regarding large number of electrons (resulting in a current of a few hundred mA) is very important due to the fact that plasma plume loses a large number of electrons at its initial stages, creating a charge imbalance within the plasma plume. The spectroscopic observation of the acceleration of ions near the sample can be explained in the light of this observation. However, prior to attempt an explanation, we shall look into the density and temperature near the sample where the acceleration of ions is observed. As described in earlier article [32], estimation of density of plasma plume at early times is performed using a high resolution spectrograph (1 m with 0.07-nm resolution) and ICCD. The spectra of neutral nickel lines were recorded and the Stark broadening parameters for these lines were estimated using the width of  $H_\alpha$  recorded for the same laser energy and background pressure [32]. The estimated density and temperature of the

TABLE II. Peaking time and respective velocities of various components at 3 mm from the sample at different background pressures and laser energy of 50 mJ.

Ion or Neutral	Pressure (0.1 mbar)	Pressure (10 mbar)	Pressure (20 mbar)
Fast ion peak time	135 ns	145 ns	150 ns
Fast ion velocity	$2.2 \times 10^6 \text{ cms}^{-1}$	$2.1 \times 10^6 \text{ cms}^{-1}$	$2.0 \times 10^6 \text{ cms}^{-1}$
Fast ion energy	148 eV	135 eV	122 eV
Slow ion peak time	400 ns	350 ns	315 ns
Slow ion velocity	$7.5 \times 10^5 \text{ cms}^{-1}$	$8.6 \times 10^5 \text{ cms}^{-1}$	$9.5 \times 10^5 \text{ cms}^{-1}$
Slow ion energy	17.2 eV	22.6 eV	27.6 eV
Neutral peak time	375 ns	450 ns	405 ns
Neutral velocity	$8 \times 10^5 \text{ cms}^{-1}$	$6.6 \times 10^5 \text{ cms}^{-1}$	$7.4 \times 10^5 \text{ cms}^{-1}$
Neutral peak energy	19.6 eV ns	13.3 eV	16.7 eV

plasma parameter at early stage of plume evolution (200 ns) were  $N_e = 1 \times 10^{18}/\text{cc}$  and temperature of 2–3 eV as reported earlier [32].

As commonly adopted, the observation of enhancement in the speed of ionic species as well as that of neutrals can be explained using the concept of double-layer (DL) or multi-layer formation in the plasma, as discussed in a few earlier experimental and theoretical works [28,41]. It is noticed that due to the presence of relativistic electrons produced in laser-plasma interaction, significant charge separation occurs within the plasma. Due to the property of shielding, this charge separation is possible within a few Debye lengths, which is known as the thickness of the double layer. It is assumed that within the plasma, at a very small distance (few times the Debye length) [41], a large electric field is generated. This electric field can accelerate/decelerate the ions/electrons based on the polarity. Plasma will try to restore the charge neutrality by reorganizing the charged species [28]. Due to the escape of fast electrons, a region is formed within the plasma where quasi-neutrality is broken as the ions trail the electrons. In this scenario the ions from the core region of plasma can be accelerated to establish quasineutrality. Due to the large mass of accelerated ions, the core region can have less number of ions and an inverse process of deceleration is also possible.

For a plasma with density of the order of  $10^{18}/\text{cc}$  and temperature of 2–3 eV, Debye length is estimated to be around 10 nm, and the possible thickness for DL can be assumed to of the order of few Debye lengths (say, 100 to 1000 nm). From the negative peak observed for ion saturation current and the oscillations on floating potential, it can be assumed that the electrons escape from the plasma with moderate to high velocity (minimum  $10^8 \text{ cm/s}$  it is expected that certain minimum time is required to get the hot electrons generation as the laser pulse is of 10 ns duration and the hot electrons generated have to get through the film which is in the process of melting). In addition to the hot electrons, we also have to consider the possibility of thermal electrons generated from the ablation of the film which escape. At the same time, it can also be noted that the laser intensity may not be sufficient to generate relativistic electrons as reported in Refs. [8,9,13] with the experiments using ultrafast lasers. In earlier experiments with comparable laser fluences at ns pulse width, the acceleration of ions is observed at longer distances using charge collector diagnostics at relatively higher pressures ( $6.8 \times 10^{-2} \text{ mbar}$ ) [28]. In our experiment the maximum fluence used is  $21 \text{ Jcm}^{-2}$

(100 mJ) and a background pressure of 20 mbar and have observed acceleration of ionic species as well as neutral even at closer distance (up to 3 mm). The present experimental configuration (rear ablation geometry of thin film) is expected to be helpful in generating higher plasma density and also the generation of fast electrons from the plasma as observed in the TLP. The rigid thin film at the front side and glass substrate on the rear side confines the initial nickel plumes until the duration of complete melting of the film (few tens of nanoseconds). During this time, the high density plasma plume absorbs energy from laser light through IB, which heats up the plume and positively contributes to the generation of fast electrons by TBR and IB as discussed in Sec. III C.

The DL formation mechanism by the loss of fast electrons has been reported by Bulgakova *et al.* [28]. At this stage pictorial explanation (Fig. 8 of Ref. [28]) of formation of DL or multilayer appears to be a plausible model to explain the observation of fast ions and neutrals we observed. Figure 6 shows the acceleration of ionic peaks as the background pressure increases from 0.1 to 10 mbar and 20 mbar for 100 mJ energy. Tables II and III list the peaking times of these peaks for different background pressures for 50 and 100 mJ excitation. In addition to the peaking time, the average velocities and the corresponding energies are also listed in these tables. However, it has to be noted that the expansion of plasma species into the background gas involves interaction of plume with background gas molecules and hence free expansion can not take place. Even, at lowest pressure (0.1 mbar) used in the present work, free expansion of the plume is not likely occur. Hence, the actual instantaneous velocity could be much higher than what is listed in these tables. The objective of this table is limited to highlight the change in velocity for different species with ambient gas pressure and hence to provide the estimate of an approximate value of electric field responsible for this increase in velocity. The striking difference between our results and that reported in reference [28] is the way the background effect the evolution of ionic species. In their case, the ion acceleration was slowed whereas we found that background gas increases it. As will be discussed, the probable reason for this could be the presence of microfields.

The peak timing values for slow ions and neutrals at 0.1 mbar and 100 mJ are almost the same (410 ns Table III), which corresponds to a velocity of  $7.3 \times 10^5 \text{ cms}^{-1}$ . Assuming no significant acceleration or deceleration for this slow peak, the velocity of ions and neutrals can be assumed to

TABLE III. Peaking time and respective velocities of various components at 3 mm from sample at different background pressures and laser energy of 100 mJ.

Ion or neutral	Pressure (0.1 mbar)	Pressure (10 mbar)	Pressure (20 mbar)
Fast ion peak time	145 ns	145 ns	155 ns
Fast ion velocity	$2.1 \times 10^6 \text{ cms}^{-1}$	$2.1 \times 10^6 \text{ cms}^{-1}$	$1.9 \times 10^6 \text{ cms}^{-1}$
Fast ion energy	135 eV	135 eV	110 eV
Slow ion peak time	410 ns	315 ns	280 ns
Slow ion velocity	$7.3 \times 10^5 \text{ cms}^{-1}$	$9.5 \times 10^5 \text{ cms}^{-1}$	$10.7 \times 10^5 \text{ cms}^{-1}$
Slow ion energy	16.3 eV	27.6 eV	35.0 eV
Neutral peak time	410 ns	390 ns	380 ns
Neutral velocity	$7.3 \times 10^5 \text{ cms}^{-1}$	$7.7 \times 10^5 \text{ cms}^{-1}$	$7.9 \times 10^5 \text{ cms}^{-1}$
Neutral peak energy	16.3 eV ns	18.1 eV	19.1 eV

be the same as the initial velocity. At 20 mbar, the slow ion peak advances to 280 ns corresponding to a velocity of  $10.7 \times 10^5 \text{ cms}^{-1}$ . Here it should be noted from Table III that the velocity of neutrals also increases with pressure for 100 mJ excitation. However, the drag of background gas can be seen for lower energy where the velocity of neutrals decreases. The change in velocity of neutrals or ions can be attributed to the combined effect of acceleration attained from the DL and the drag force of the background medium throughout the distance it travels. here for the ease of estimation of acceleration gained by the nickel ions, the drag force is ignored. The estimation of the electric field produced within the DL and the acceleration it generates is estimated as described by Eliezer *et al.* [42]. Taking the velocity of slow neutrals at 0.1 mbar as the initial velocity (not accelerated), and 1000 nm ( $10\text{--}100 \times \lambda_D$ ) as the DL thickness, the acceleration of ions responsible for increasing the velocity of the slow peak to  $10.7 \times 10^5 \text{ cms}^{-1}$  at 20 mbar (where maximum acceleration is seen) is estimated as  $3 \times 10^{15} \text{ cms}^{-2}$ . To attain this acceleration for singly charged nickel ion, the electric field required is estimated as  $1.8 \times 10^9 \text{ Vcm}^{-1}$ . A similar estimation performed for other energies and background pressures also gets a value of electric field within one order of magnitude lower than the highest observed field. In this work, the observed values of electric field generated within the plume are rather high considering the fluence range we are using. The earlier reported [13,43] values of DL fields also are of this order, though, at a much higher laser energy. This anomalous behavior will be discussed in the Sec. III D considering the effect of microfields produced in the plume.

### C. Recombination process and generation of fast electrons

The formation of DL in plasma is explained with the concept of formation of hot electrons, by getting additional energy from the plasma plume. The major processes responsible for this can be three-body recombination (TBR) [44] and IB absorption [45]. In TBR, the electron is recombined to an ion to some excited level and can transfer the excess energy to another electron. Harilal *et al.* [46] observed that TBR dominates radiative recombination for higher density and lower temperatures. In our case the temperature is not very high. It is likely that TBR increases the electron energy at a longer distance. TBR (which has a rate proportional to  $T^{-9/2}$ ) is more prominent at lower temperature and higher densities.

The radiative recombination (which has a rate proportional  $T^{-3/4}$ ) is also to be dominating at lower temperatures but less as compared to TBR [44,46,47]. As estimated in Ref. [46] the three-body recombination dominates if the density  $N_e \geq \frac{3 \times 10^{19} T_e^{15/4}}{Z} m^{-3}$  where  $T_e$  expressed in eV and Z is the charge state. In the present scenario, where the density is measured as  $2 \times 10^{18} \text{ cm}^{-3}$  (for higher pressure and close to the sample and at a delay of 200–300 ns) and the temperature estimated is in the range of 2–3 eV, three-body recombination will be the dominant mechanism for recombination. The absorption of energy from the incident laser through IB is also expected to have hot electrons generated. In fact, laser of 1064 nm with longer pulse width is a favorable case for IB heating.

As mentioned, the density close to the sample at a delay of 200 ns is measured as  $2 \times 10^{18} \text{ cm}^{-3}$  using Stark width and the temperature at 10 mm is measured using TLP as 1.5 eV. If interpolating these values with existing understanding and the observations elsewhere, then it can be assumed that the plasma at an early stage will have higher density and temperature than the measured values at later times and longer distances. Hence, with the help of NIST data base [33] we can estimate the extent of ionization. At a density of  $10^{18} \text{ cm}^{-3}$  and a temperature of 3 eV, as in the case of initial state of the plume, the plasma will be completely ionized and will have negligible neutral contribution ( $3.5 \times 10^{-3}\%$ ). However, as the temperature and density fall down to  $10^{17} \text{ cm}^{-3}$  and 1 eV, respectively, as happens the case of expanding plasma plume, there will be significant amount of neutrals (6.5%) present in the plasma. This information is helpful in assuming that the observed neutrals at early stages of plasma evolution are formed by the recombination of ions and hence have almost the same velocity profile as that of ions. For the recombination process, the density and temperature range of initial plasma plume will be favorable for TBR, fast electrons will be generated which may leave the plasma plume and generate a charge imbalance resulting in the electric field as discussed in Sec. III B.

### D. Asymmetry in spectral emission—Presence of microelectric field

The spectral shape of 712.22 nm line [ $3d^9(^2D_{5/2})4p \rightarrow 3d^9(^2D)4p$ ] of neutral nickel recorded using high-resolution spectrometer in the range of few 100 ns appears to show a large asymmetric broadening as the background pressure

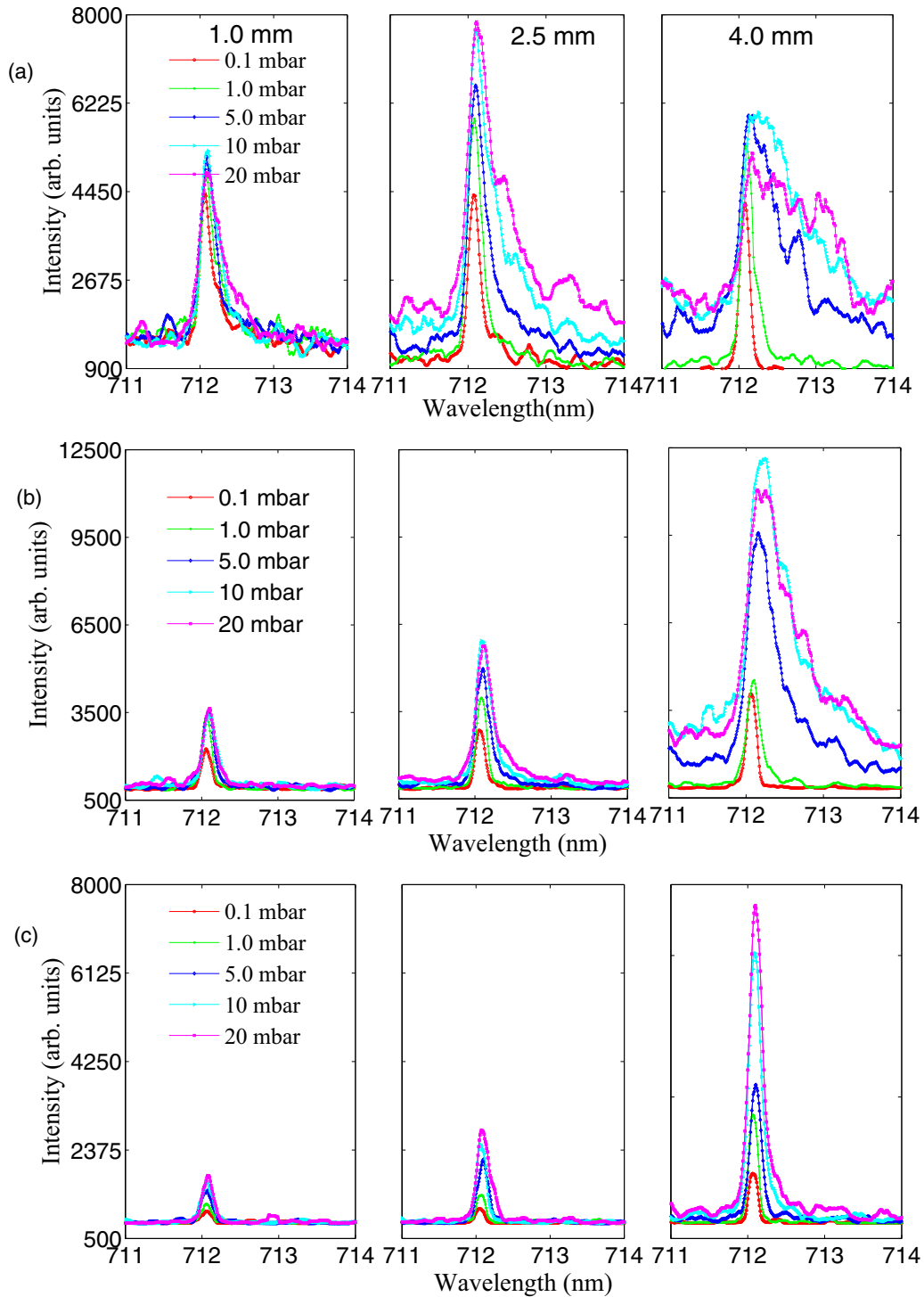


FIG. 13. Asymmetric broadening of 712.22 nm neutral line of nickel at nearer points for delay times of (a) 200 ns, (b) 300 ns, and (c) 500 ns for different background pressures and laser energy of 100 mJ.

increases. Figure 13 shows the spectral shape of this line at different background pressures and for three spatial positions for three different delay times (200, 300, and 500 ns). Figure shows that the spectral line is broadened asymmetrically towards the red and asymmetry increases with pressure. The NIST database shows that there is no other strong emission line present for nickel (even for ions) near the red region with significant transition probability. Hence, the asymmetric

broadening can be interpreted considering some perturbation in atomic levels for this specific transition.

Interestingly other neutral lines recorded in the present work with different upper energy levels do not exhibit such asymmetry. As a particular transition involves different emitting levels and some are likely to be perturbed significantly in the presence of field and hence may be reflected by certain lines. A detailed study pertaining to

different atomic transitions will be attempted in future for asymmetric broadening. However, present results clearly demonstrate that 712.22-nm line exhibits significant asymmetric broadening.

As can be seen from the figure, asymmetry is strongly correlated with the spatial position and plume evolution time. For instance, at 200 ns for almost all the background pressures, asymmetry appears identical at a distance very close to the sample 1.0 mm. However, as the distance increases a significant variation in asymmetry is observed with increase in background pressure. Figure 13(a) shows evolution of asymmetry with background pressure at 2.5 mm, where no significant asymmetry in spectral shape is seen for 0.1 mbar of background pressure. However, a large asymmetrical broadening can be seen at 20 mbar of background pressure. As the time increases to 500 ns [Fig. 13(c)], the spectral broadening is smallest and no significant asymmetry is observed. Considering these facts we can rule out the collisional broadening with increase in pressure.

The asymmetry ( $A_s$ ) of spectral broadening at a width of  $\Delta\lambda$  can be expressed using a simple formula [48],

$$A_s(\Delta\lambda) = \frac{I_R - I_B}{I_R + I_B}, \quad (1)$$

where  $I_R$  and  $I_B$  are the line intensities at wavelength separation of  $\Delta\lambda$  and  $-\Delta\lambda$  from the line center, respectively. A positive value of  $A_s$  is indicative of an asymmetry towards the red wavelength and a negative value corresponds to the asymmetry towards blue region. Figure 14 shows the calculated  $A_s$  [Fig. 14(a)] and the respective FWHM [Fig. 14(b)] for three distances at delay time of 200 ns for a laser energy of 100 mJ [spectra shown in Fig. 13(a)]. As can be seen from Fig. 14(a), the asymmetry is increase with background pressure and maximum asymmetry is observed at 4.0 mm from the sample. From Fig. 14(b), at 4 mm the FWHM of the spectral line also higher as compared to other locations, an observation seen in earlier reports [32] for the emission of other nickel lines as well.

The experimental observations indicate the role of plasma density for spectral asymmetry as the rest of parameters like laser fluence, pulse width and wavelength, etc. remain the same in this experiment. The variation in background pressure in the range of few mbar is also not expected significantly influence the spectral shape due to pressure broadening. As already reported [32], with increase in background pressure the plasma density also increases substantially due to the confinement of plasma plume considering the drag nature of background medium, which peaks around 4–6 mm. Hence, the asymmetry observed in this experiment can be correlated with enhanced density of plasma and the spectroscopic properties of the particular line which shows asymmetry.

Such asymmetry in spectral line shape has been reported in literature [49–51], however with, very limited experimental data and the cause of the asymmetry has been attributed to the “generated microelectromagnetic fields” (ion microfield). In the present scenario where we observe a significantly large acceleration for the ionic species and resulting neutral species generated due to recombination, observation of asymmetry of this neutral line is further underlining the pos-

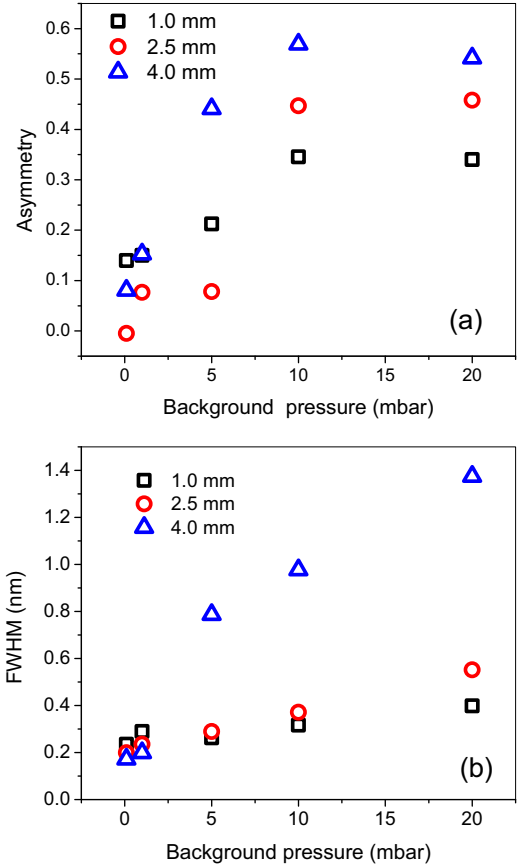


FIG. 14. Asymmetry of 712.22 nm neutral line of nickel estimated as per Eq. (1) and the FWHM of the same line for 200 ns delay for different background pressures and distance up to 4.5 mm for laser energy of 100 mJ.

sibility of the presence of significant electric field. Assuming the ion microfield (possibly due to density and temperature gradients) is the origin of asymmetry of the neutral line profile, the observed asymmetry suggests the existence of such fields. Hence, the acceleration observed for the plasma species (ions and neutrals) with increase in background pressure, appears to be a continuous process, and hence the assumption of acceleration occurring only in the DL (of width having a few times  $\lambda_D$ ) may not be a valid assumption. We believe that simultaneous observation of ion acceleration and asymmetric broadening seen in the present work of neutral line is interesting and to some extent explains the observed acceleration.

#### IV. SUMMARY

In conclusion, the present study bring out some new interesting features in the optical time of flight spectra of neutral and ionic nickel. The results clearly demonstrate that ions are accelerated considerably. A double layer concept for ion acceleration seems to be inadequate as the retrieved electric field is anomalously higher. The results indicate the presence of microelectric fields which may result in large acceleration. Moreover, the background pressure substantially modifies the microelectric fields. The observed behavior in ion acceleration

coupled with the fact that there is large asymmetry in a particular neutral line (712.22 nm) which varies with distance and time points towards the evolution of microelectric fields inside plasma plume. The effect of acceleration observed on ion species also reflects in neutral emission also confirming that the neutrals are formed by the recombination process. The formation of fast neutrals due to recombination is also confirmed by the fact that it is prominent in one of the observed neutral

lines (712.22 nm). We believe these observations have not been reported in laser produced plasma experiments within the intensity range of present experiment.

Although, finer detailed experiments and modeling may shed more light on the observed acceleration of ionic species in this configuration, the present study brings out interesting features of ionic and neutral dynamics in rear ablation of nickel plasma plume in the rear ablation geometry.

- 
- [1] H. Daido, M. Nishiuchi, and A. S. Pirozhkov, *Rep. Prog. Phys.* **75**, 056401 (2012).
- [2] E. G. Gamaly, *Femtosecond Laser-Matter Interaction Theory, Experiments and Applications* (CRC Press, Boca Raton, FL, 2011).
- [3] L. Torrioni, F. Caridi, L. Giuffrida, A. Torrioni, G. Mondio, T. Serafino, M. Caltabiano, E. Castrizio, E. Paniz, and A. Salici, *Nucl. Instrum. Methods Phys. Res., Sect. B* **268**, 1657 (2010).
- [4] T. Tajima and G. Mourou, *Phys. Rev. ST Accel. Beams* **5**, 031301 (2002).
- [5] T. Brabec, *Strong Field Laser Physics*, Physics and Astronomy (Springer, Berlin, 2009).
- [6] S. Gammino, L. Torrioni, L. Andò, G. Ciavola, L. Celona, L. Láska, J. Krasa, M. Pfeifer, K. Rohlena, E. Woryna, J. Wolowski, P. Parys, and G. D. Shirkov, *Rev. Sci. Instrum.* **73**, 650 (2002).
- [7] R. Rajeev, T. Madhu Trivikram, K. P. M. Rishad, V. Narayanan, E. Krishnakumar, and M. Krishnamurthy, *Nat. Phys.* **9**, 185 (2013).
- [8] M. Chen, A. Pukhov, T.-P. Yu, and Z.-M. Sheng, *Plasma Phys. Controlled Fusion* **53**, 014004 (2010).
- [9] N. Iwata, K. Mima, Y. Sentoku, A. Yogo, H. Nagatomo, H. Nishimura, and H. Azechi, *Phys. Plasmas* **24**, 073111 (2017).
- [10] X. F. Shen, B. Qiao, H. Zhang, Y. Xie, S. Kar, M. Borghesi, M. Zepf, C. T. Zhou, S. P. Zhu, and X. T. He, *Appl. Phys. Lett.* **114**, 144102 (2019).
- [11] C. Scullion, D. Doria, L. Romagnani, A. Scattoni, K. Naughton, D. R. Symes, P. McKenna, A. Macchi, M. Zepf, S. Kar, and M. Borghesi, *Phys. Rev. Lett.* **119**, 054801 (2017).
- [12] H. W. Powell, M. King, R. J. Gray, D. A. MacLellan, B. Gonzalez-Izquierdo, L. C. Stockhausen, G. Hicks, N. P. Dover, D. R. Rusby, D. C. Carroll, H. Padda, R. Torres, S. Kar, R. J. Clarke, I. O. Musgrave, Z. Najmudin, M. Borghesi, D. Neely, and P. McKenna, *New J. Phys.* **17**, 103033 (2015).
- [13] A. Maksimchuk, S. Gu, K. Flippo, D. Umstadter, and V. Y. Bychenkov, *Phys. Rev. Lett.* **84**, 4108 (2000).
- [14] S. Bulanov, T. Esirkepov, V. Khoroshkov, A. Kuznetsov, and F. Pegoraro, *Phys. Lett. A* **299**, 240 (2002).
- [15] H. Hora, *Laser Part. Beams* **25**, 37 (2007).
- [16] S. H. Glenzer, B. J. MacGowan, P. Michel, N. B. Meezan, L. J. Suter, S. N. Dixit, J. L. Kline, G. A. Kyrala, D. K. Bradley, D. A. Callahan, E. L. Dewald, L. Divol, E. Dzenitis, M. J. Edwards, A. V. Hamza, C. A. Haynam, D. E. Hinkel, D. H. Kalantar, J. D. Kilkenny, O. L. Landen *et al.*, *Science* **327**, 1228 (2010).
- [17] L. Torrioni, *Nukleonika* **60**, 207 (2015).
- [18] P. H. Bucksbaum, R. R. Freeman, M. Bashkansky, and T. J. McIlrath, *J. Opt. Soc. Am. B* **4**, 760 (1987).
- [19] V. Sazegari, M. Mirzaie, and B. Shokri, *Phys. Plasmas* **13**, 033102 (2006).
- [20] L. Láska, S. Cavallaro, K. Jungwirth, J. Krása, E. Krouský, D. Margarone, A. Mezzasalma, M. Pfeifer, K. Rohlena, L. Rýč, J. Skála, L. Torrioni, J. Ullschmied, A. Velyhan, and G. Veronarinati, *Eur. Phys. J. D* **54**, 487 (2009).
- [21] M. Passoni, L. Bertagna, and A. Zani, *New J. Phys.* **12**, 045012 (2010).
- [22] J. Badziak, S. Głowacz, S. Jabłoński, P. Parys, J. Wołowski, H. Hora, J. Krása, L. Láska, and K. Rohlena, *Plasma Phys. Control. Fusion* **46**, B541 (2004).
- [23] A. P. L. Robinson, M. Zepf, S. Kar, R. G. Evans, and C. Bellei, *New J. Phys.* **10**, 013021 (2008).
- [24] S. S. Bulanov, E. Esarey, C. B. Schroeder, S. V. Bulanov, T. Z. Esirkepov, M. Kando, F. Pegoraro, and W. P. Leemans, *Phys. Plasmas* **23**, 056703 (2016).
- [25] N. Farid, S. S. Harilal, H. Ding, and A. Hassanein, *J. Appl. Phys.* **115**, 033107 (2014).
- [26] S. Amoroso, R. Bruzzese, N. Spinelli, and R. Velotta, *J. Phys. B: At., Mol. Opt. Phys.* **32**, R131 (1999).
- [27] R. P. Singh, S. L. Gupta, and R. K. Thareja, *Phys. Plasmas* **20**, 123509 (2013).
- [28] N. M. Bulgakova, A. V. Bulgakov, and O. F. Bobrenok, *Phys. Rev. E* **62**, 5624 (2000).
- [29] R. F. Wood, K. R. Chen, J. N. Leboeuf, A. A. Puretzky, and D. B. Geohegan, *Phys. Rev. Lett.* **79**, 1571 (1997).
- [30] S. Amoroso, B. Toftmann, and J. Schou, *Phys. Rev. E* **69**, 056403 (2004).
- [31] R. Wood, J. Leboeuf, K. Chen, D. Geohegan, and A. Puretzky, *Appl. Surf. Sci.* **127-129**, 151 (1998).
- [32] J. Thomas, H. C. Joshi, A. Kumar, and R. Philip, *Phys. Plasmas* **25**, 103108 (2018).
- [33] A. Kramida, Yu. Ralchenko, J. Reader, and NIST ASD Team, NIST Atomic Spectra Database (ver. 5.5.6): <https://physics.nist.gov/asd> (National Institute of Standards and Technology, Gaithersburg, MD, 2018).
- [34] S. S. Harilal, C. V. Bindhu, M. S. Tillack, F. Najmabadi, and A. C. Gaeris, *J. Phys. D: Appl. Phys.* **35**, 2935 (2002).
- [35] S. Harilal, *Appl. Surf. Sci.* **172**, 103 (2001).
- [36] S. Harilal, B. O'Shay, Y. Tao, and M. Tillack, *J. Appl. Phys.* **99**, 083303 (2006).
- [37] S. Mahmood, R. S. Rawat, M. S. B. Darby, M. Zakauallah, S. V. Springham, T. L. Tan, and P. Lee, *Phys. Plasmas* **17**, 103105 (2010).
- [38] N. A. Gatsonis, L. T. Byrne, J. C. Zwahlen, E. J. Pencil, and H. Kamhawi, *IEEE Trans. Plasma Sci.* **32**, 2118 (2004).

- [39] A. Kumar, R. K. Singh, J. Thomas, and S. Sunil, *J. Appl. Phys.* **106**, 043306 (2009).
- [40] S. Gurlui, M. Agop, P. Nica, M. Ziskind, and C. Focsa, *Phys. Rev. E* **78**, 026405 (2008).
- [41] S. Eliezer and H. Hora, *Fusion Technol.* **16**, 419 (1989).
- [42] S. Eliezer, E. Kolka, and H. Szichman, *Laser Part. Beams* **13**, 441 (1995).
- [43] S. Eliezer and H. Hora, *Phys. Rep.* **172**, 339 (1989).
- [44] W. Griffith, *J. Fluid Mech.* **31**, 826 (1968).
- [45] R. L. Morse and C. W. Nielson, *Phys. Fluids* **16**, 909 (1973).
- [46] S. S. Harilal, T. Sizyuk, A. Hassanein, D. Campos, P. Hough, and V. Sizyuk, *J. Appl. Phys.* **109**, 063306 (2011).
- [47] E. Hinnov and J. G. Hirschberg, *Phys. Rev.* **125**, 795 (1962).
- [48] B. T. Vujičić, S. Djurović, and J. Halenka, *Z. Phys. D* **11**, 119 (1988).
- [49] H. R. Griem, *Plasma Spectroscopy* (McGraw-Hill, New York, 1964).
- [50] A. M. EL Sherbini, A. E. EL Sherbini, and C. G. Parigger, *Atoms* **6**, 44 (2018).
- [51] E. Oks, *Atoms* **6**, 50 (2018).